BiOBr/MoS2 catalyst as heterogenous peroxymonosulfate activator toward organic pollutant removal: Energy band alignment and mechanism insight

ZHANG, Bofan, ZHANG, Mutian, ZHANG, Liang, BINGHAM, Paul <http://orcid.org/0000-0001-6017-0798>, TANAKA, Manabu, LI, Wen and KUBUKI, Shiro

Supporting Information

BiOBr/MoS_2 catalyst as heterogenous peroxymonosulfate activator toward organic pollutant removal: Energy band alignment and mechanism insight

Bofan Zhang[1, *], Mutian Zhang[2], Liang Zhang[3], Paul A. Bingham[4], Wen Li[2, *], Shiro Kubuki[1]

[1]Department of Chemistry, Tokyo Metropolitan University, Tokyo 192-0397, Japan

[2]School of Material Science and Engineering, Ocean University of China, Qingdao, China

[3]College of Chemical Engineering, China University of Petroleum, Qingdao, China

[4]College of Business, Technology and Engineering, Sheffield Hallam University, Howard Street, Sheffield S1 1WB, UK

S1. Chemicals

Bismuth nitrate hydrate, thiourea, ammonium molybdate, potassium bromide, Rhodamine B (RhB), Methylene Blue (MB), Methylene Orange (MO), Congo Red (CR), potassium dichromate, phenol, Polyvinylpyrrolidone (K-30), p-benzoquinone, methanol were purchased from Siyaku Chemical Reagent Co., Ltd., Japan. All reagents and chemicals were analytical-grade reagents without further purification.

S2. Synthesis of MoS_2 catalyst

The MoS_2 was prepared using a hydrothermal method. First, 0.58 g of ammonium molybdate and 0.532 g of thiourea were dissolved in 35 mL deionized water, and magnetically stirred for 120 min. Then, the mixture was transferred into a Teflon lined stainless steel autoclave (50 mL) and maintained at 180℃ for 24h. Finally, the product was washed with deionized water several times, and then vacuum dried at 80℃ for 6h.

S3. Characterization

The X-ray diffraction (XRD) patterns detected by X-ray diffractometer with Cu K_α radiation were applied to evaluate the crystal structure of the samples. The Fourier transform-infrared (FT-IR) spectra were tested using FT-IR optical spectrometer (Nexus 670) with KBr pellet in the range of 500-3500 cm^{-1}. The morphology and composition of BiOI were analyzed by scanning electron microscopy (SEM), transmission electron microscopy (TEM, JEM-3200FS) and TEM-energy-dispersive X-ray spectroscopy (EDX). Surface electronic states were recorded by X-ray photoelectron spectroscopy (XPS, VG MultiLab 2000) with a monochromatic Cu K_α source. The UV-vis diffusive reflectance spectra (DRS) of samples were analyzed on a UV-vis spectrophotometer. Photoluminescence (PL) spectra were obtained by

fluorescence spectrometry (FP-6300). Electrochemical impedance spectroscopy (EIS) and Mott-Schottky were analyzed in a three-electrode system of the CHI-600E electrochemical workstation (Shanghai Chenhua, China).

S4. Details of the analysis of pollutants

- Phenol: Measured by UV-vis and HPLC (C18 column 5 μm, 150 mm*4.6 mm). The mobile phase consisted of Methanol and water (80:20, v/v) at a flow rate of 0.8 mL/min with the detection wavelength at 280 nm. The column temperature was held at 25 ± 0.5 °C.
- Bisphenol A: Measured by UV-vis with the detection wavelength at 278 nm.
- Carbamazepine: Measured by UV-vis with the detection wavelength at 285 nm.
- Organic dyes: Measured by UV-vis with the detection wavelength at 554 nm for Rhodamine B (RhB); 665 nm for Methylene Blue (MB); 464 nm for Methylene Orange (MO); 498 nm for Congo Red (CR).
- Heavy metal Hexavalent chromium Cr(VI): Measured via the method of Diphenylcarbazide spectrophotometry with the detection wavelength at 540 nm.

Supplementary Figures and Tables

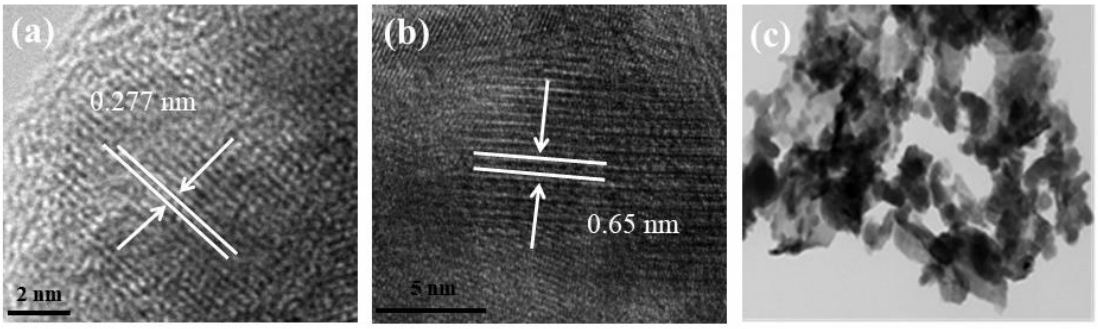

Fig. S1 TEM images of BiOBr (a), MoS_2 (b) and BMS-2 composite (c);

TEM images of BiOBr, MoS_2 and BiOBr/MoS_2 composites exhibited the stacked structure by layered aggregation of nanosheets. From the high-magnification TEM images, the continuous interplanar spacing of 0.277 nm was matched with the (001) facet in the BiOBr lattice. The lattice distance of 0.65 nm corresponded to the (002) facet of MoS_2. By using similar strategies, Xing et al. [1] in-situ synthesized an ultrathin Bi_2WO_6/Bi_2O_2S 2D-2D closely bonded heterojunction, which achieved extended light absorption and highly enhanced water splitting efficiency. Zhang et al. [2] successfully fabricated a 2D-2D bilayer junction between MoS_2 and $Bi_{12}O_{17}Cl_2$ via atomic level charge flow (Bi-S bonds), which showed ultralong carrier lifetimes and superior photocatalytic hydrogen evolution rates. Seongil et al. [3] reported a 2D p-n dichalcogenide heterojunction of α-$MoTe_2$/MoS_2 with excellent high-frequency rectification and photovoltaic capacity. Generally, the stable and strong integration between 2D BiOBr and MoS_2 could efficiently promote photogenerated charge carrier separation and transportation in the interfacial surface and improve participation in the photocatalytic process.

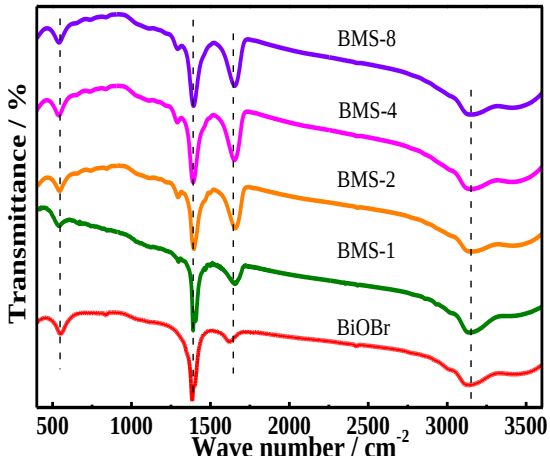

Fig. S2 FTIR analysis of BiOBr, MoS_2 and BiOBr/MoS_2 composites

The chemical structures of as-synthesized catalysts were characterized by FT-IR spectrometry. As exhibited in Fig.2b, the broader peak located at 3400-3500 cm^{-1} is attributed to the O-H stretching mode due to the water or ethanol absorbed on the catalyst surface. The absorption peak ranging from 1300-1500 cm^{-1} mainly corresponds to symmetric (v_{as}(C–O)) and asymmetric (v_s(C–O)) vibrations [4]. The characteristic peak at 1673 cm^{-1} is derived from stretching vibrations of C=O bonds. The characteristic peak about 520 cm^{-1} is attributed to the stretching vibration of Bi-O bonds [5].

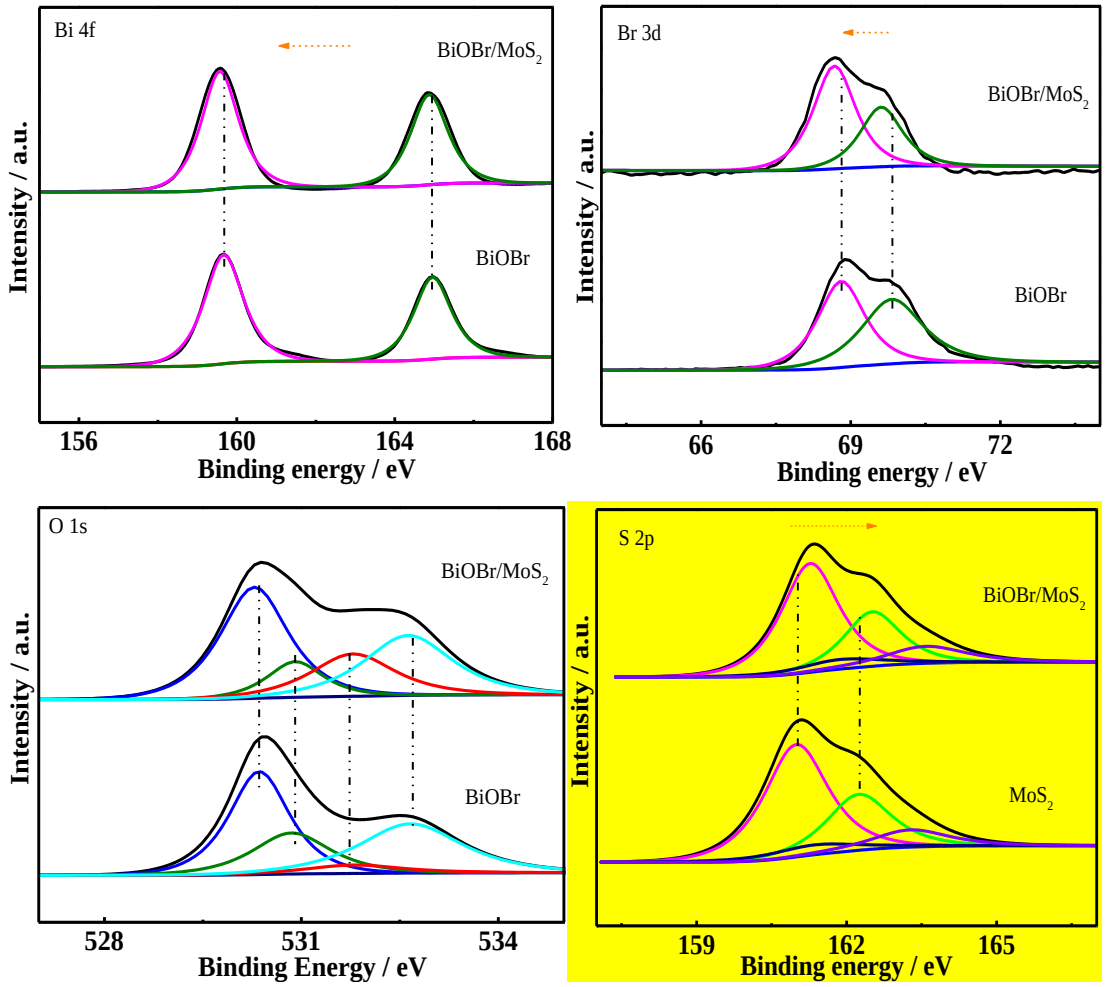

Fig. S3 XPS spectra of Bi 4f; Br 3d; O1s and S 2p in BiOBr, MoS_2 and BiOBr/MoS_2 catalyst

Table.S1 Catalyst compositions and the bonding information detected by XPS

Catalyst	Bi content (%)	Mo content (%)	Bi/Mo atomic ratio
$BiOBr/MoS_2$	18.2	1.08	16.8

The surface chemical composition and state of BiOBr, MoS_2 and $BiOBr/MoS_2$ were further characterized by X-Ray Photoelectron (XPS). The high-resolution spectral peaks of Bi 4f at 159.57 eV and 164.87 eV were identified to Bi $4f_{7/2}$ and Bi $4f_{5/2}$ electrons, indicating the state of Bi^{3+} in $BiOBr/MoS_2$ composite. Compared with pristine BiOBr, these peaks in $BiOBr/MoS_2$ exhibited a blue shift. Moreover, two characteristic peaks appearing at 68.80 eV and 69.82 eV in BiOBr were ascribed to Br $3d_{5/2}$ and Br $3d_{3/2}$ electrons, respectively. However, after combining with MoS_2, the binding energy of Br $3d_{5/2}$ and Br $3d_{3/2}$ shifted to lower value by 0.2 eV, illustrating the presence of chemical interaction between BiOBr and MoS_2. Besides, two characteristic peaks at 161.01 and 162.25 eV were identified to S $2p_{3/2}$ and S $2p_{1/2}$, respectively. Meanwhile, the coexistence of four typical peaks of S suggested the presence of 1T and 2H phase in MoS_2 catalyst. In comparation with pure MoS_2, the high resolution of S $2p_{3/2}$ and S $2p_{1/2}$ shifted to higher value by 0.2-0.3 eV in $BiOBr/MoS_2$ composites. All of these elements with shifted binding energy clearly indicated the strong electronic coupling between BiOBr and MoS_2 in the heterojunction structure. For the O 1s spectrum, the peak can be deconvoluted into four O species, which corresponded to Bi-O bonds, oxygen vacancy, C=O groups and adsorbed H_2O on the surface of catalyst, respectively [6]. Furthermore, the Bi and Mo content (Table 1) measured by XPS was similar to the experimentally theoretical ratio. The coexistence of these elements and substances in XPS spectra further evidenced the formation of $BiOBr/MoS_2$ (2D/2D) heterojunctions.

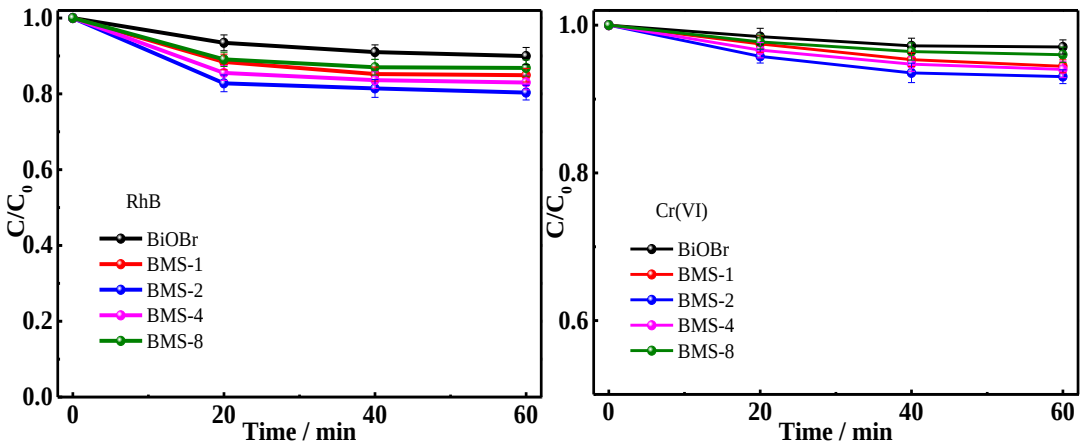

Fig.S4 The adsorption ability for RhB and Cr(VI) under dark condition

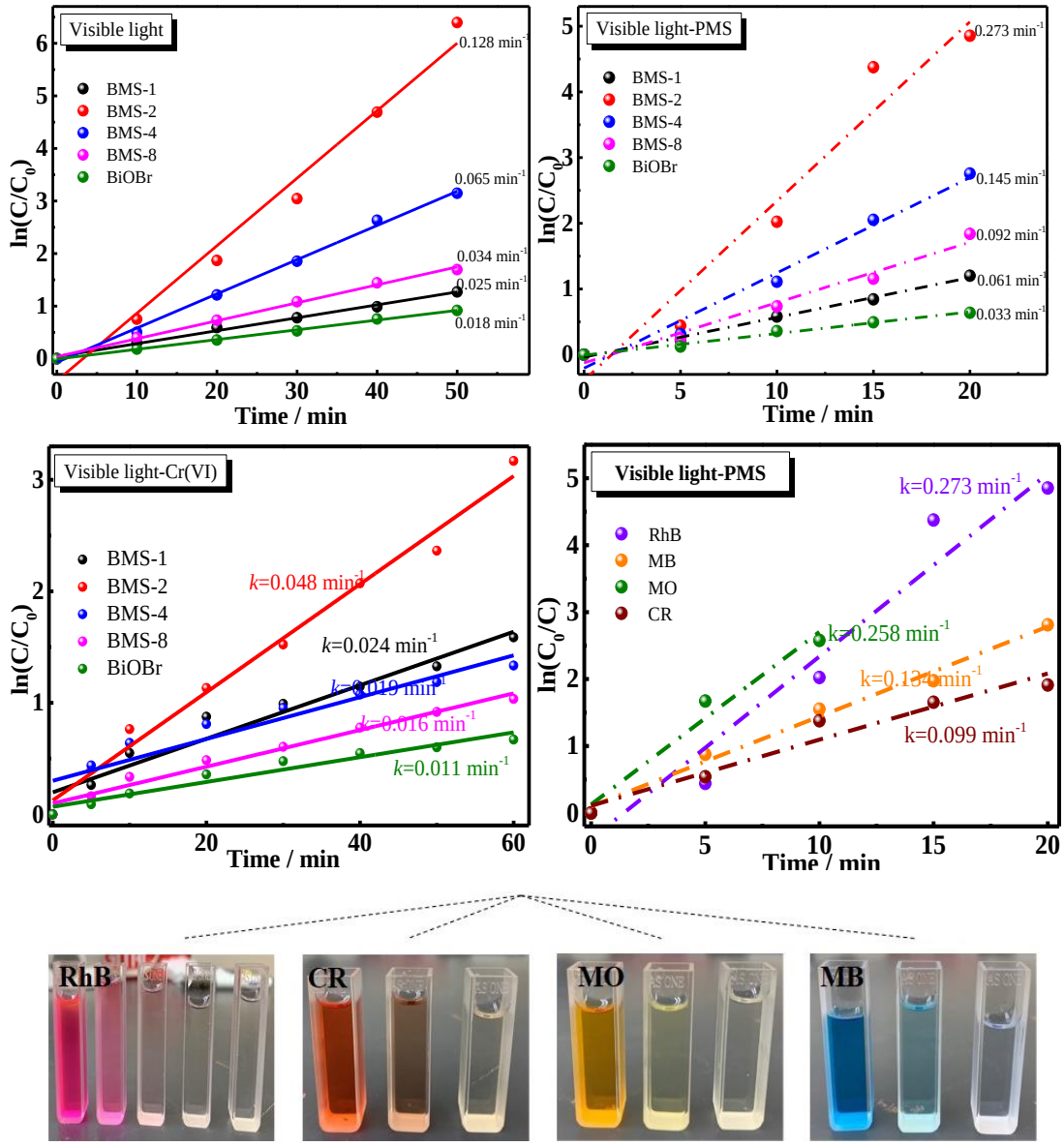

Fig. S5 Pseudo-first-order kinetics of degradation organic dyes and removal of Cr(VI) by BiOBr/MoS_2 catalysts

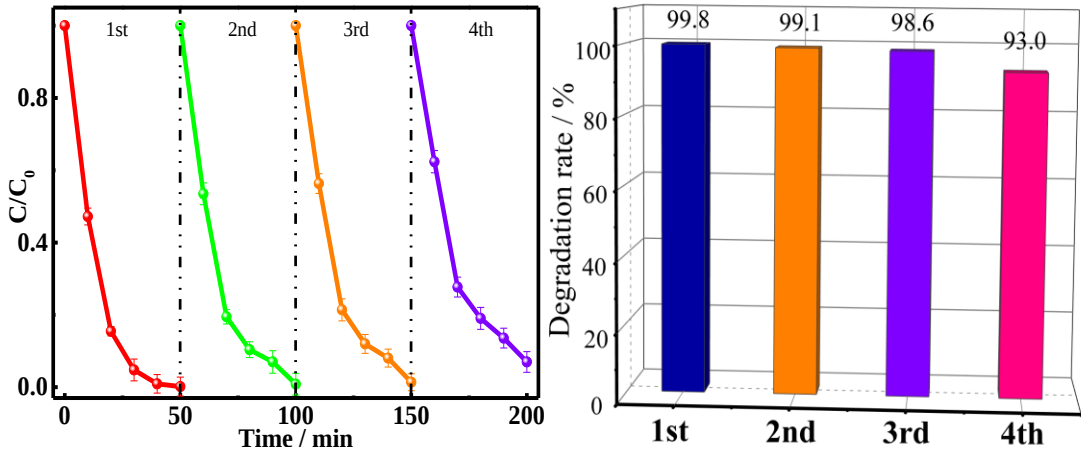

Fig. S6 Stability test for BiOBr/MoS_2 catalyst under visible light irradiation without PMS

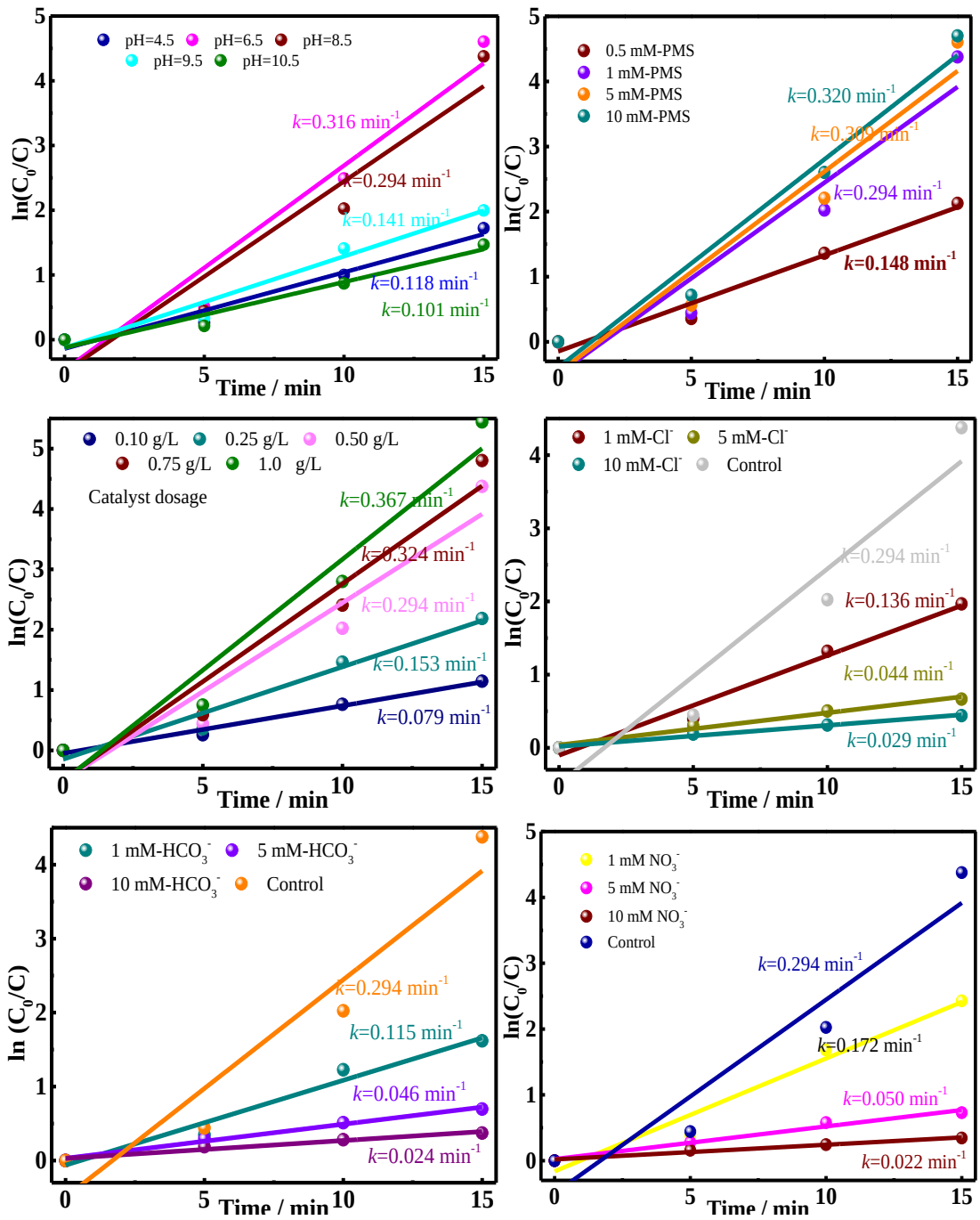

Fig. S7 Pseudo-first-order kinetics of degradation of RhB in different influencing factors of the BMS-2 catalyst

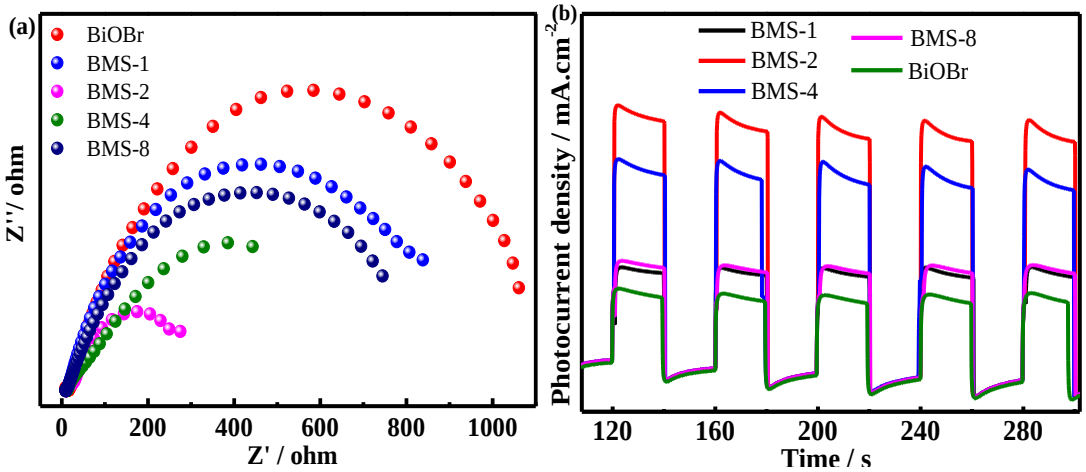

Fig.S8 (a) EIS Nyquist plot and (b) photocurrent response of as-synthesized catalysts

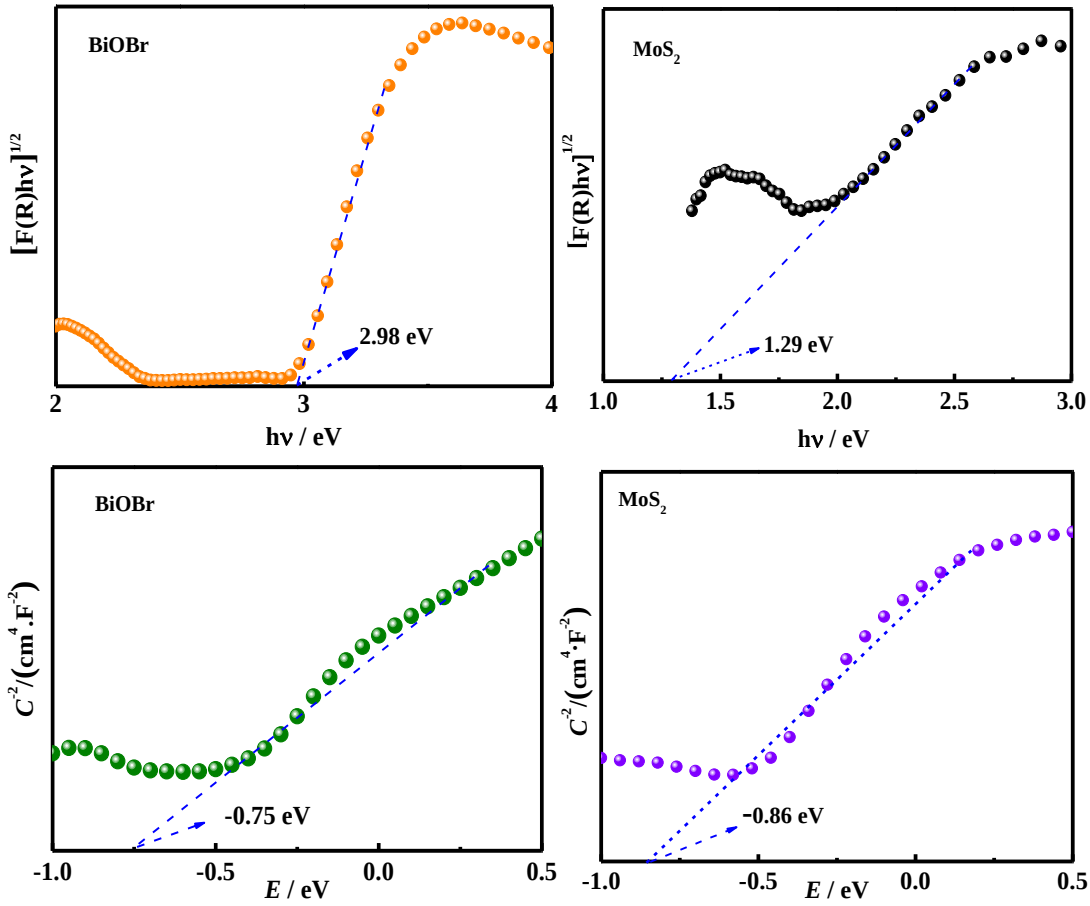

Fig.S9 Band gap energy and conduction band potential of BiOBr and MoS_2

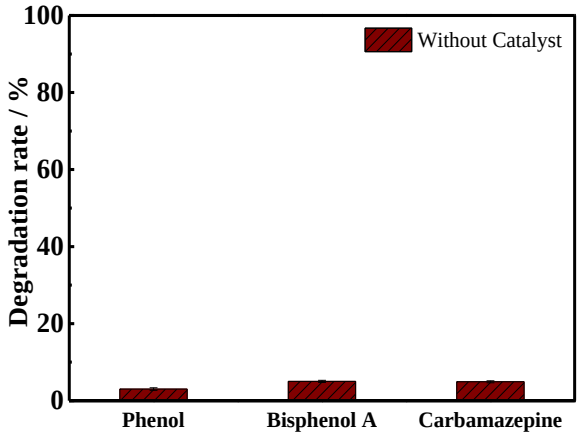

Fig.S10 The Phenol, Bisphenol A and Carbamazepine degradation without addition of catalysts

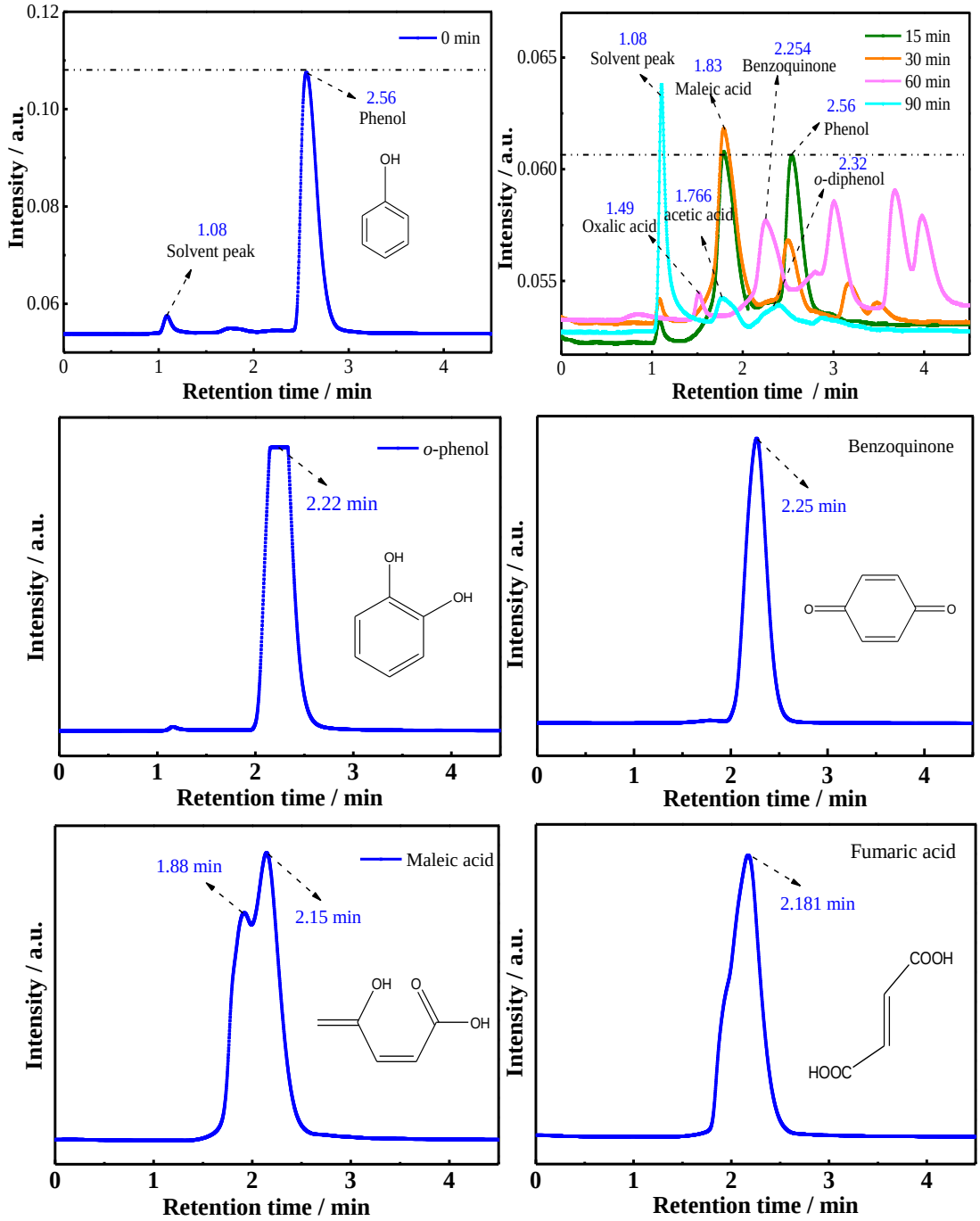

Fig. S11 HPLC chromatograms of phenol degradation at different times and showing the possible intermediates, and proposed degradation mechanism of phenol by BiOBr/MoS_2 catalyst

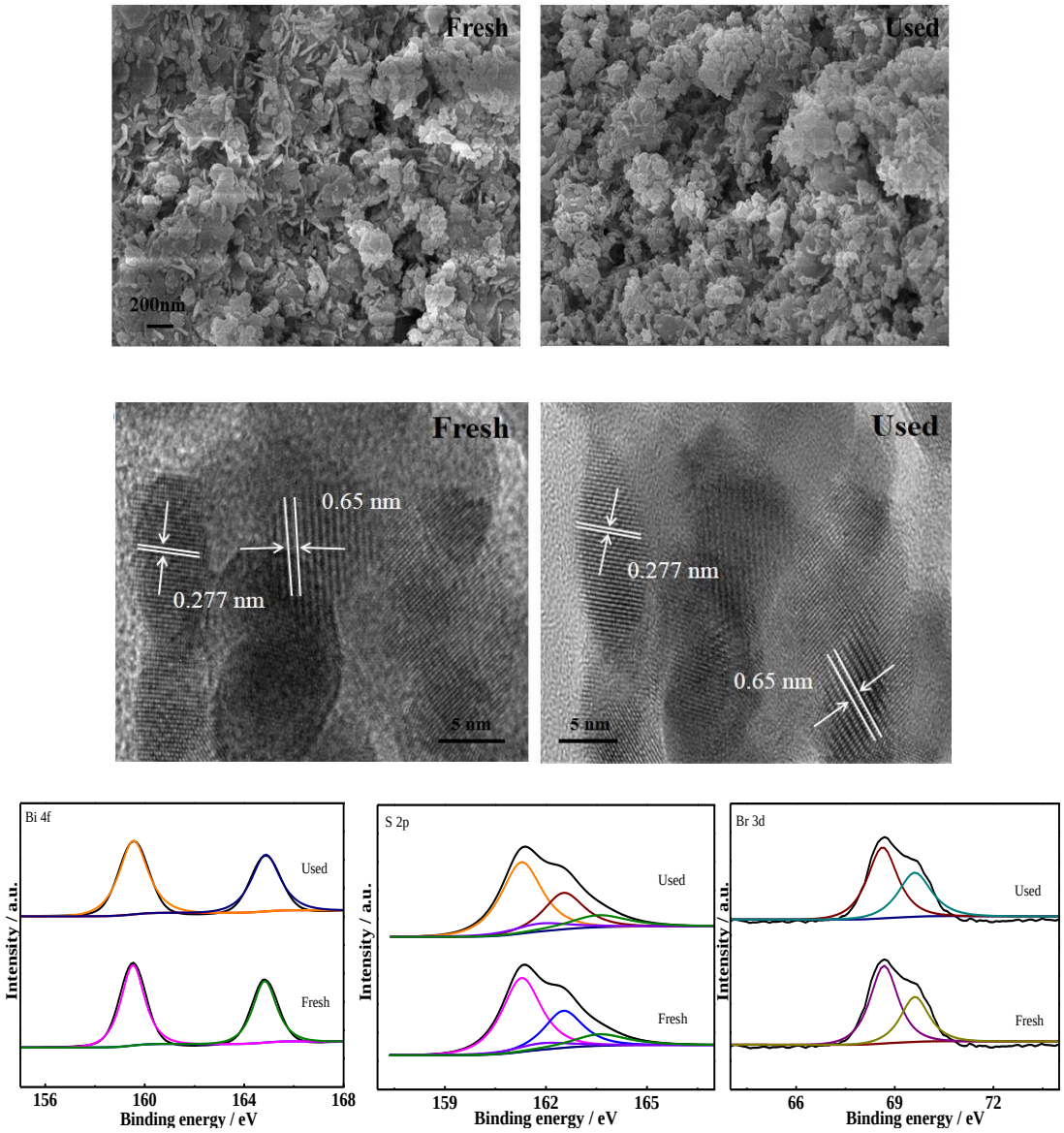

Fig. S12 SEM images, HRTEM images and XPS spectra (Bi, S, Br) of BMS-2 before and after five cycles under PMS/*hv* system

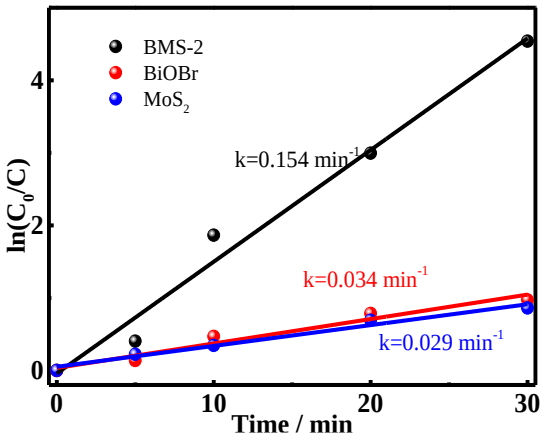

Fig.S13 Corresponding constant rate *k* of visible light-driven PMS activation for the degradation of RhB in a 3.0-L solution

Reference:

[1] Z. Xing, J. Hu, M. Ma, H. Lin, Y. An, Z. Liu, Y. Zhang, J. Li, S. Yang, From One to Two: In Situ Construction of an Ultrathin 2D-2D Closely Bonded Heterojunction from a Single-Phase Monolayer Nanosheet, Journal of the American Chemical Society, 141 (2019) 19715-19727.

[2] J. Li, G. Zhan, Y. Yu, L. Zhang, Superior visible light hydrogen evolution of Janus bilayer junctions via atomic-level charge flow steering, Nature Communications, 7 (2016) 11480.

[3] J.Y. Kwak, J. Hwang, B. Calderon, H. Alsalman, N. Munoz, B. Schutter, M.G. Spencer, Electrical Characteristics of Multilayer MoS_2 FET's with MoS2/Graphene Heterojunction Contacts, Nano Letters, 14 (2014) 4511-4516.

[4] J. Xi, H. Xia, X. Ning, Z. Zhang, J. Liu, Z. Mu, S. Zhang, P. Du, X. Lu, Carbon-Intercalated 0D/2D Hybrid of Hematite Quantum Dots/Graphitic Carbon Nitride Nanosheets as Superior Catalyst for Advanced Oxidation, Small, 15 (2019) 1902744.

[5] X. Lv, D.Y.S. Yan, F.L.-Y. Lam, Y.H. Ng, S. Yin, A.K. An, Solvothermal synthesis of copper-doped BiOBr microflowers with enhanced adsorption and visible-light driven photocatalytic degradation of norfloxacin, Chemical Engineering Journal, 401 (2020) 126012.

[6] Q. Zhang, J.-B. Liu, L. Chen, C.-X. Xiao, P. Chen, S. Shen, J.-K. Guo, C.-T. Au, S.-F. Yin, An etching and re-growth method for the synthesis of bismuth ferrite/MIL-53(Fe) nanocomposite as efficient photocatalyst for selective oxidation of aromatic alcohols, Applied Catalysis B: Environmental, 264 (2020) 118529.